出力は0.3[mW]とした．レーザの照射対象は，大脳皮質(ブタ)，白質 (ブタ)，及び血液(ラット)とした．血液に関しては，実際の手術中，脳表面に血液がたまっている状態を模擬するため，ファントム上に血液を浸し実験を行った．ファントムは，寒天に散乱体であるイントラリピッドを混ぜ，630[nm]におけるグリオーマの散乱係数$\mu_s'=3[\mathrm{cm}^{-1}]$に調整したものを用いた[3)4)]．血液層の厚さは，0.25[mm]，0.5[mm]，0.75[mm]，1[mm]，1.25[mm]，1.5[mm]とした．また，ガイドレーザを対象の鉛直上から照射し，CCD カメラはそれに対し60[°]の角度から観測することとした．実験は室内の蛍光灯照明下で行った。シャッター速度(1/1000，1/2000，1/4000，1/10000)，Y 閾値(0～250，5 ポイント刻み)を変化させ計測を行った．

結果を **Fig.1** に示す．スポットが消失してしまう限界のラインを，閾値の上限値，ノイズが画面全体に現れ始めるラインを閾値の下限値とした．

大脳皮質，白質に関しては，532[nm]のレーザの場合閾値を最高(1/10000，250)にしてもスポットの抽出は可能であった（Fig.1(b)）．635[nm]レーザは532[nm]の場合よりスポット抽出が困難であった（Fig.1(c,d)）．血液ファントムではスポットの強度が弱く，1/4000 以下のシャッタースピードでなければスポット抽出ができなかった・・・（Fig.1(a)）．閾値の下限値はいずれの場合もY=35 となった（Fig.1(e)）．

3．2輝度閾値とフォーカシング誤差評価

実験の際，スポットの抽出を行った後，スポットの重心座標の算出も行ったところ，輝度の閾値を低くするほど，フォーカシングの誤差が大きくなる傾向が見られた.これは，閾値を下げるほど，より組織の奥で散乱した光を検出してしまうためである.

そこで，散乱係数をそれぞれ$\mu_s'=3$，30[cm^{-1}](グリオーマや血液に近い値として3[cm^{-1}]，大脳皮質や白質に近い値として30[cm^{-1}]を設定)に調整したイントラリピッドのファントムを用い，輝度閾値を下げることにより生じるフォーカシングの誤差を計測した.

結果を **Fig.2** に示す．横軸はスポットの面積[pixel^2]である.輝度閾値を下げると抽出されるスポットの面積も大きくなるが，この面積とフォーカシングの誤差との間に相関が見られた.散乱係数が低いほうが，誤差も大きくなることが分かった.

4．考察及びまとめ

Fig.1から1/4000以下のシャッタースピードであれば，適切な輝度閾値を設定することで，組織の状態によらずガイドレーザのスポットが抽出できる可能性が示された.また閾値が低くなるにつれ抽出されるスポットの面積が大きくなることで，フォーカシングに与える誤差も大きくなった.以上より，閾値を動的に変化させるといった工夫が必要であると考えられる.

本研究の一部はテルモ科学技術振興財団・文部科学省科学研究費（＃15700349）による.

文献

1) 大森繁他. コンピュータ制御による脳外科レーザー処置の実験的検討. 第 12 回日本コンピュータ外科学会大会論文集 2003; 33-34

2) 野口雅史他. 脳腫瘍治療レーザ手術装置用オートフォーカス機構の開発　第2報. 第12回日本コンピュータ外科学会大会論文集 2003; 35-36

3) Sterenborg HJ et al: The spectral dependence of the optical properties of the human brain. Lasers Med Sci 4: 221-227: 1989

4) Van Staveren, JM Moes, Jan Van Marle, A Prahl, Van Germert: Light scattering in Intralipid-10% in the wavelength range of 400-1100 nm. Appl. Opt. 30: 4507-4514: 1991

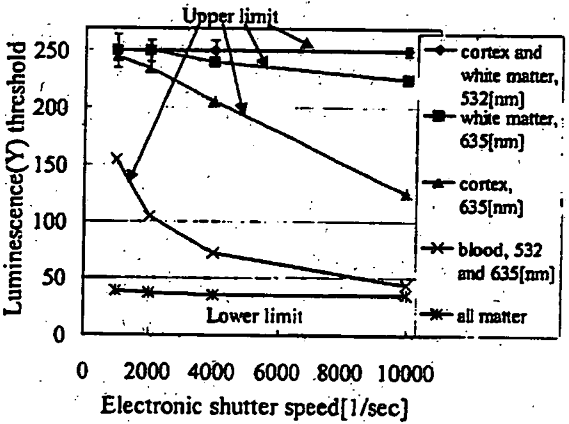

Fig.1 Upper and lower limit of each threshold

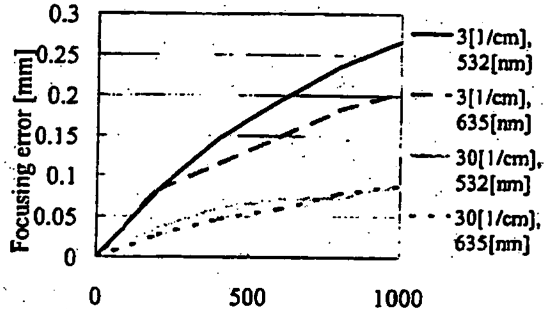

Fig.2 Relationship of the Area of the spot and focusing error

System Design for Implementing Distributed Modular Architecture to Reliable Surgical Robotic System

Eisuke Aoki[1], Takashi Suzuki[1], Etsuko Kobayashi[1], Nobuhiko Hata[1],
Takeyoshi Dohi[2], Makoto Hashizume[3], and Ichiro Sakuma[1]

[1] Institute of Environmental Studies, Graduate School of Frontier Sciences, The University of Tokyo
http://bme.pe.u-tokyo.ac.jp/index_e.html
{aoki, t-suzuki, etsuko, sakuma}@miki.pe.u-tokyo.ac.jp
[2] Graduate School of Information Science and Technology, The University of Tokyo
noby@atre.t.u-tokyo.ac.jp
dohi@miki.pe.u-tokyo.ac.jp
[3] Department of Disaster and Emergency Medicine, Kyushu University
mhashi@dem.med.kyushu-u.ac.jp

Abstract. A method that resolves the two competing requirements for a surgical robotic system (reliability and scalability) is discussed, along with its preliminary implementation in a master-slave system. The proposed method enables an architecture that can be scaled without impairing the performance of the surgical robotic system. Our method uses an optimized architecture consisting of two components: a common object request broker architecture (CORBA) and a master-slave system that typically operates using two-way communication links between a client and a remote server (the dedicated system architecture). In this new architecture, the surgical robotic system can maintain a reliable performance and can integrate with various systems in a transparent manner, regardless of the hardware, operating system, or programming language. Our method was evaluated by recording all the available surgical information, and shows a reliable scalability for a surgical robotic system requiring real-time operation, regardless of the condition of the components of a CORBA-based system.

1 Introduction

Many telerobotic systems using distributed modular architectures have been developed over the last few years. The advantages of using network-based systems built on top of distributed computing systems technology are the reduction in system costs, the arbitrary location of clients, dynamic access to remote expertise as required, and the decreased costs of operator training. Following the current trends in modern distributed system design, open reconfigurable and scalable architectures can be built using standard middleware software for distributed object computing. As one of several standard middleware software packages available, many studies using surgical robotic systems have been reported

C. Barillot, D.R. Haynor, and P. Hellier (Eds.): MICCAI 2004, LNCS 3217, pp. 184–191, 2004.

employing the common object request broker architecture (CORBA) package [1,2]. CORBA uses an Object Request Broker (ORB) as the middleware that establishes a client/server relationship between objects. The client can invoke a method on the server object across a network in a transparent manner without knowing where the application servers are located, or what programming language and operating system are being used. In addition, the components of a CORBA-based system can be implemented and run independently to implement the application, and can be easily integrated into new systems. Schorr et al. reported on the application of a CORBA system to control an image-guided surgical robot, where they controlled an MRI-compatible biopsy robot by sending the control information using CORBA [3,4]. However, there have been several reports that CORBA is not always an effective, flexible, and robust technique for Internet-based robotics systems. One of the technological problems associated with CORBA is how to guarantee stable and reliable control under interference from a CORBA system. Generally, real-time software is required to control mechatronic systems, such as robots, and to develop a stable and reliable control system under limited computational resources, it is important to evaluate the overall system load imposed on the computer system. However, in the distributed modular architecture of a computer aided surgical system, where the system configuration may change depending on the clinical requirements, it is difficult to estimate the system load before the design of the system. In recent years, a master-slave manipulator system has been applied to less-invasive laparoscopic surgery [5]. In contrast to an image-guided control system, the master-slave manipulator system is a relatively slow imaging system, and it requires a higher control frequency. On the other hand, to realize safe and accurate surgical operation, the integration of a surgical navigation system employing a master-slave surgical manipulator is necessary, and for this purpose, a distributed modular architecture is desirable. Thus, it is important to design a control system that meets these two competing requirements, and we set out to resolve these two competing requirements (scalability and reliability) in our surgical robotic system. This paper describes the following system components.

1. The use of an optimized architecture consisting of two components: a dedicated system architecture and CORBA, and
2. The development of an intermediate system to resolve any interference occurring between two architectures.

The above allow a surgical robotic system to maintain a reliable performance and to integrate various systems in a transparent manner, regardless of the hardware, operating system, or programming language used.

2 System Architecture

2.1 System Overview

It is important for a system to have sufficient computational power to handle the necessary information during processing. However, even if a system has sufficient performance, in general, it cannot handle situations that occur at random.

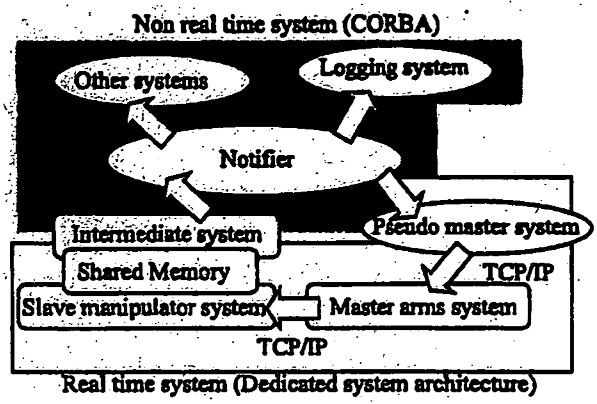

Fig. 1. System architecture

A system needs to function stably under such circumstances, and for the stable transmission of data using a CORBA-based system, the synchronous transmission of data is desirable for reliable communication among distributed objects. It is very difficult to define priorities for multiple objects connected to each other, unless the real time performance of the subsystems is well defined. In the case of a computer-aided surgery system, the configuration of the system may change, depending on the clinical requirements of specific cases. In the design of our prototype system, we prepared an intermediate system that allowed adjustments between the real time master-slave manipulator system and the CORBA-based system to be made. The system we developed consisted of a control system designed for real time control of the surgical master-slave manipulator system, a CORBA-based system that realized a distributed modular architecture, and an intermediate software system that connected these two systems(Fig. 1).

2.2 A Master-Slave Manipulator System with a Dedicated Communication System

The master-slave manipulator system consisted of a pair of master arms (MASTER) and a slave manipulator system (SLAVE). In the MASTER system(Fig. 3), an operator sits in front of a monitor showing a laparoscopic view and controls the master manipulators, using footswitches to command the SLAVE. The SLAVE system uses three slave robotic manipulators with seven degrees of freedom that include a grasping function, and an endoscope with a variable viewing angle [6,7]. The slave robotic manipulators are located on passive positioning arms for easier presetting of the manipulators before surgical operation. The position and orientation of the manipulators and the endoscope were measured using a Polaris optical positioning sensor (Northern Digital Inc., http://www.ndigital.com). The motion of the master arms was recognized as

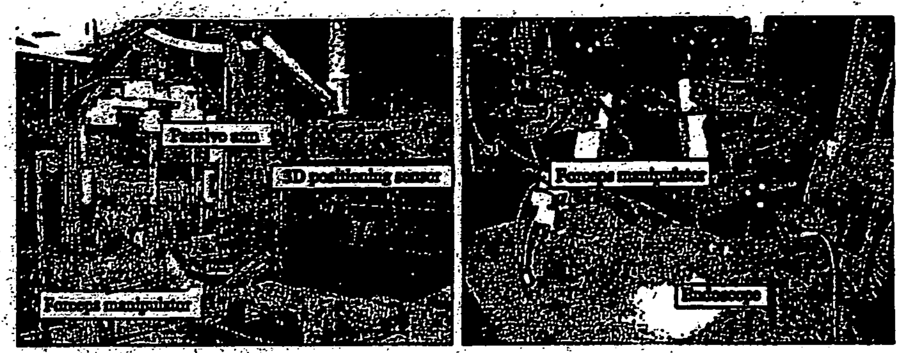

Fig. 2. Surgical slave manipulator system

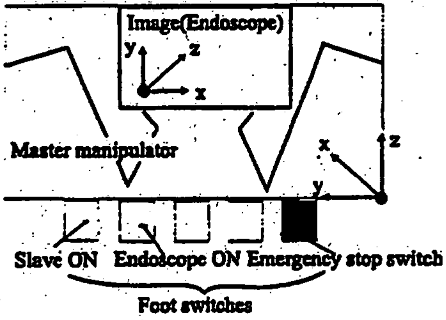

Fig. 3. Master arms system

the motion commands of the endoscope's coordinates, and this motion was transformed to the manipulator's coordinates. The required computation for the SLAVE control was conducted using a real time base. The MASTER and SLAVE were connected using a dedicated communication channel employing TCP/IP protocol. These two systems were tightly connected as a single client device and a server robot. As an alternative to the MASTER, a pseudo-MASTER could be used that could store the time series data from the master arms' motion and related control information, and could relay this data to the SLAVE. The pseudo-MASTER was also connected with the SLAVE using a dedicated communication channel, and in addition, this system was connected to the other distributed objects using CORBA. Using this pseudo-MASTER, the SLAVE could accept motion commands from the other objects using CORBA.

2.3 Common Object Request Broker Architecture (CORBA)

CORBA defines a framework for developing distributed applications. As many implementations support different operating systems, we chose the Adaptic Communication Environment (ACE) and the Object Request Broker (TAO) developed by Washington University, USA [8]. The developed system uses a CORBA-based system to interface with the distributed objects in the system. As an example of a distributed object that could be connected to the master-slave manipulator system, we implemented a logging system that recorded time-series data for the following control information:

- Commands from the master arm system to the slave manipulator system: the position and orientation of the master-manipulators and foot switches (On and Off).
- The status of the slave manipulators: position and orientation of the slave manipulators.
- The viewing direction of the endoscope.
- The set position of the slave manipulators: The set position of each passive arm holding the slave manipulator (the three slave manipulators, endoscope, and Polaris 3-D positioning sensor).

2.4 Intermediate System

We prepared an intermediate system located between the master-slave manipulator system and the communication system using CORBA software. The intermediate system receives data from the master-slave manipulator system in an asynchronous manner by means of a shared memory. It then sends the data to the other objects using CORBA in a synchronous manner to make the communication reliable. Introduction of this intermediate system loosely connected the master-slave manipulator system and the communication system using CORBA software. It prevented any interference with the robot control system due to instantaneous decrease of the system performance caused by communication overload and communication errors. Using this intermediate system, we were able to maintain the performance of the master-slave manipulator system and ensure the reliability of the entire system while keeping connectivity to the communication system based on CORBA. The developed system is shown in Figure 4. To evaluate the system stability under operating conditions, the proposed system design was subjected to the following tests using the experimental conditions shown in Figure 4.

- Logging the system using the proposed system design.
- Carrying out the master-slave experiment using a communication rate of 100 msec.
- Using the total recorded surgical information for evaluation.

3 Results and Discussion

We implemented the system described in Section 2, shown in Figure 4, and we conducted experiments in operating the master-slave surgical manipulator

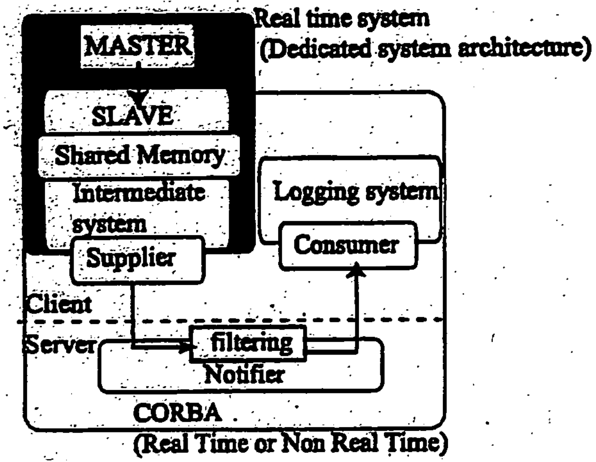

Fig. 4. System architecture in experiment

system. We also recorded the time-series data from the control data of the manipulators using CORBA in the logging system. We could successfully operate the master-slave manipulator and were able to record the control data without any problems. Figure 5 shows examples of the recorded data from the manipulator motion. Figures 5(a) and 5(b) show the position of the slave manipulator. The manipulator was only activated when the foot switch was activated. The data shows the expected behavior of the slave manipulator. Figure 5(c) shows the change in joint angle during operation. We also tested the system without the intermediate system connecting the communication system based on CORBA and the real time control system for the master-slave manipulator in place. Synchronous transmission was used in these experiments to maintain reliable communication. Under these conditions, the real time control system for the manipulator suffered from the influence of coexisting processes of the CORBA communication system, resulting in an unstable system operation. By reinserting the intermediate system, we could successfully interact with the communication processes of CORBA with real time control of the manipulator. The data stored in the logging system was also transferred to the pseudo-master system, and used to repeat the same recorded motions of the manipulator. The slave manipulator repeated the same motions in a stable manner. In the application of the system in a computer aided surgery environment, distributed objects in the system will not always be in a real time system. If we adopt a system with close connections that require a strict real time operation, such as manipulator control, then these non-real time objects can form a bottleneck that will determine the overall system performance. Schorr et al. reported the application of a CORBA-based system to control an image guided surgical robot. They controlled an MRI-compatible biopsy robot by sending its control information

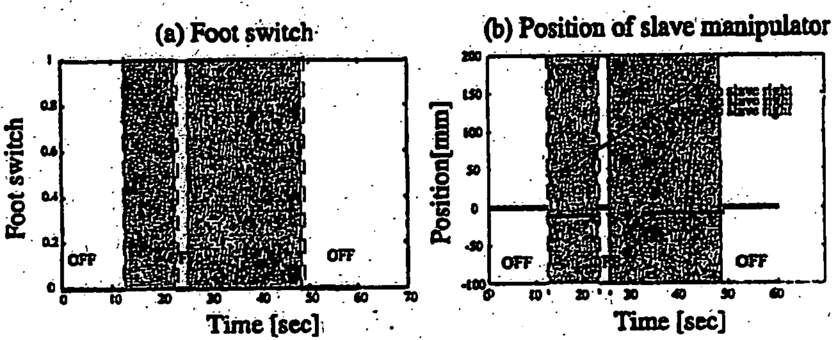

(a) Foot switch

(b) Position of slave manipulator

(c) Joint angle of slave manipulator

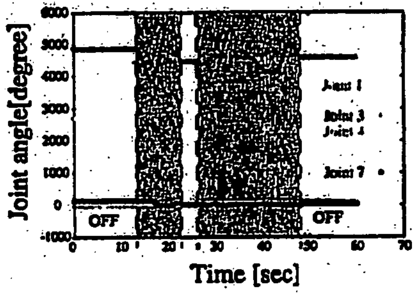

Fig. 5. Log data of logging system;(a)Foot switch, (b)Position of the slave manipulator, (c)Each joint angle of slave manipulator

using CORBA [3,4]. Considering the nature of an MRI scanner, it seems that the required bandwidth for communicating navigation data in that case is not as high as the bandwidth requirements for communicating to our master-arms and slave-manipulators or for the dynamic motion control of our robotic manipulators. Thus, it is effective to utilize CORBA as the communication interface. When we combine the master-slave manipulator system for less invasive surgery, or for a surgical navigation system or surgical simulation system, then in general, the required transmission frequency of the navigation data is not so high. On the other hand, the scalability of a system that allows for the connection of various types of intraoperative imaging devices and instrumentation with positional data is more important. From this consideration, we propose the use of the intermediate system that will compensate for differences in the required real time performance among the distributed objects, while maintaining a reliable and extendable data communication at relatively low frequency using CORBA.

4 Conclusion

We have proposed a method to resolve the two competing requirements of a surgical robotic system: scalability and reliability, and we have shown the following:

- Our system design combined real time objects, such as a master-slave manipulator control system with other non-real time objects used in a computer-aided surgical assistance system. With the proposed system design, the reliability and stability of real time systems and scalability of a CORBA-based system were realized at the same time.
- We developed an intermediate system with real time and asynchronous processing to compensate for the real time and non-real time nature of the distributed objects. This system enabled the coexistence of the dedicated system architectures required for real time processing and CORBA.
- As an example of this function, we developed a logging system for the motion control data from the manipulators and a pseudo master system for the manipulator operation. We confirmed the stable real time control of the surgical master-slave manipulator together with data communication to the other distributed objects.

In future work, we will incorporate a surgical navigation system using the master-slave surgical robotic manipulator to realize safe and accurate surgical operation of this system.

References

1. SONGMIN JIA and KUNIKATSU TAKASE. Internet-based robotic system using corba as communication architecture. *Journal of Intelligent and Robotic Systems*, 34:121–134, 2002.
2. A.Pernozzoli, C.Burghart, J.Brief, S.Habfeld, J.Raczkowsky, J.Muhling, U.Rembold, and H.Worn. A Real-time CORBA Based System Architecture for Robot Assisted Craniofacial Surgery. In *Medicine Meets Virtual Reality 2000 J.D. Westwood et al. (Eds.) IOS Press, 2000*, 2000.
3. A. Bzostek, R.Kumar, N.Hata, O. Schorr, R. Kikinis, and R. H .Taylor. Distributed Modular Computar-Integrated Surgical Robotic Systems:Implementation using modular software and network systems. In *proc, MICCAI '00*, pages 969–978, 2000.
4. Oliver Schorr, Nobuhiko Hata, Andrew Bzostek, Rajesh Kumar, Catherina Burghart, Russel H. Taylor, and Ron Kikinis. Distributed Modular Computar-Integrated Surgical Robotic Systems:Architecture for Intelligent Object Distribution. In *proc, MICCAI '00*, pages 979–987, 2000.
5. G.H.Ballantyne. Robotic surgery,telerobotic surgery,telepresence,and telementoring. In *Springer-Verlag New York Inc.*, pages 1389–1402, 2002.
6. Takashi Suzuki, Eisuke Aoki, Etsuko Kobayashi, Takayuki Tsuji, Kozo Konishi, Makoto Hashizume, and Ichiro Sakuma. Development of forceps manipulator for assisting laparoscopic surgery. In *proc of CARS*, page 1338, 2004.
7. Takemasa Hashimoto, Etsuko Kobayashi, Ichiro Sakuma, Kazuhiko Shinohara, Makoto Hashizume, and Takeyoshi Dohi. Development of wide-angle view laparoscope using wedge prisms. *Journal of Robotics and Mechatronics*, pages 129–137, 2004.
8. David Levine and Sumedh Mungee. The design and performance of real-time object request brokers. *Computer Communications*, 21, 1998.

04(XI)-77

CORBAを用いたプラットフォーム下における リアルタイム非同期通信によるパフォーマンスの評価

青木 英祐[1], 鈴木 孝司[1], 小林 英津子[1], 波多 伸彦[2], 土肥 健純[2],
小西 晃造[3], 橋爪 誠[3], 佐久間 一郎[1]
東京大学大学院 [1]新領域創成科学研究科, [2]情報理工学系研究科,
[3]九州大学大学院 医学研究院 災害・救急医学

The Evaluation of system performance using a Distributed Modular Architecture by real-time asynchronous communication

[1]E.Aoki, [1]T.Suzuki, [1]E.Kobayashi, [2]N.Hata, [1]T.Dohi, [3]K.Konishi, [3]M.Hashizume, [1]I.Sakuma
[1]Graduate School of Frontier Sciences, [2]Graduate School of Information Science and Technology, The University of Tokyo.
[3]Disaster and Emergency Medicine, Graduate School of Medical Science, Kyushu University.

Abstract: As a mean of integration technology, Common Object Request Broker Architecture (CORBA) has became popular. Use of CORBA make it possible to integrate various systems in a transparent manner, regardless of the hardware, operating system, or programming language. However, there have been some problems, for example such as interference between systems on integrating various systems. To solve this problem, there is a method using asynchronous communication between systems. With this method, transferring some data between systems becomes less reliable because the communication occurs at random. Therefore, the method of solving these problems is required. In this research, we describe following two components: 1) Implementation the method of real-time asynchronous communication when each system transmits data. 2) Development of logger system for evaluation of system performance. The evaluation of system performance showed that the method was effective to keep performance on a CORBA.

Key Words: laparoscopic surgery, medical robot, master-slave system, CORBA, realtime system, system architecture

1. 背景

近年，低侵襲手術が広まるに従い，ナビゲーションシステム，ロボットマニピュレータシステム，術中・術後の事故の原因究明を行うために，術中の記録を行うシステムなど様々な術者支援システムの研究が盛んに行われており，その効果が期待されている．将来的には，これらのシステムを統合した統合支援プラットフォーム下での術者支援が望まれている．統合プラットフォームは個々のシステムから構成され，システム間の連携による術者支援が行われる．そのため，データ受け渡しの形態によっては，パフォーマンスの低下を生む恐れが生じている[1]．統合を行う技術として Common Object Request Broker Architecture System(以下 CORBA)を用いたシステムが近年盛んに研究されている[2]．CORBA を用いることで，OS やソフトウェアの変更や，接続先の変更によるネットワーク設計の変更を最小限に抑えること可能である．しかし，TCP/IP に比べて通信負荷が大きくなることや同期処理を用いたデータ受け渡しの際に，システム間のパフォーマンスの依存関係が問題となっている．これを解決するための，非同期処理を行うシステム下で確実なデータの受け渡しを行うことは，各システムの処理がランダムであるため困難である．

そこで本研究では，腹部手術支援ロボットシステムを対象とした手術支援統合プラットフォーム下において，ロボットマニピュレータのパフォーマンスを確保しつつ，術者操作記録等のデータの収集を行う Logger の開発を行った．また，その評価としてパフォーマンスの測定実験を行ったので報告する．

2．システム構成

2.1 全体のシステム構成

全体のシステムは，マスタシステム（以下マスタ)、患者に対して手術を行うスレーブシステム（以下スレーブ)，マスタ・スレーブでの操作記録を行う Logger から構成されている．マスタとスレーブは TCP/IP による同期処理によりデータの受け渡しが行われている．また，スレーブと Logger との情報の受け渡しに，Intermediate system を設け，中間的にデータの受け渡しを行っている．

2.2 Intermediate system

一般的に統合システム下では，システム間に同期処理を用いることで，データの確実な受け渡しと時間の同期を取ることができるが，相互のパフォーマンスに大きく依存するため，非同期にて受け渡しを行う必要がある．通常のOS(Windows,Linux など)の非同期処理によるデータの受け渡しでは，すべての処理が OS に依存しているためログが落ちる場合が生じる．そのため，非同期かつ時系列にて確実にデータのストックを行うことが要求される．Intermediate system はマスタ・スレーブ間の情報をストックする機能，リアルタイム処理により，確実に決められた周期で Notifier へ送信する機能，非同期処理により Consumer である Logger へ受け渡す機能を持つ．リアルタイム OS(以下：RT)として TimeSysLinux® (TimeSys Corporation)を利用し，CPU リソースの割り当てと周期実行により，他のタスクに依らず一定の時間間隔にてデータの送信を行うシステムを実現している．

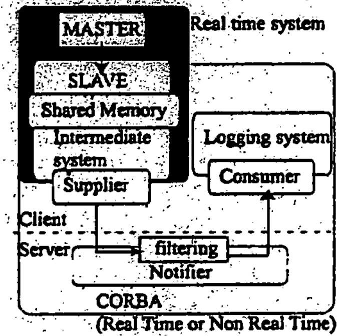

Fig.1 System image overview: Client application implements Supplier (Master, Slave system Intermediate system) or consumer module(Logger)

3. 評価実験

3.1 実験方法

Figure.1に示す実験システムを構築し，Supplier からNotifierへそしてまた，Loggerへと情報を送信した．Loggerで記録するデータとしてマスタ・スレーブにおける操作情報を時系列にて記録した．それにより，Intermediate systemのRT環境および非RT環境下の変化によるデータの比較評価を行った．パフォーマンスの基準はデータの取得が確実に行えたかどうかである．そのためLoggerで取得するログの情報の先頭に番号を割り振り，その番号が順番どおり取得できたかの評価を行った．RT環境下での設定条件として,CPUリソースの割り当てを30[msec]の周期で60[%]割り当て,30[msec]のリアルタイム周期実行にてNotifierへのログの送信を行った．

3.3 実験結果および考察

Figure.2 に示すように非 RT 環境では RT 環境に比べ，パフォーマンスの違いが大きく見られた．この理由として，Logger へのデータ送信時間にばらつきが生じたことや，マルチタスク処理を行っているスレーブシステムにおいては予期せぬ他のプロセスの影響を受けたことが考えられる．この影響を CPU リソースの割り当てにより回避しパフォーマンスが大きく向上可能であることが示されている．様々なシステムが非同期にて接続される統合システム下において，データの受け渡しにリアルタイム処理を施すことで大きな効果が期待できると考えられる．

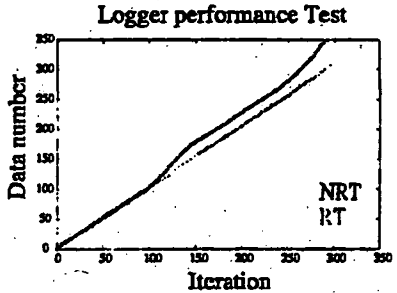

Fig.2 Comparing the performance between RT and NRT. (The vertical axis shows the recorded data number, the horizontal axis shows the loop number of system)

4. おわりに

本稿では統合プラットフォームとして CORBA を用い，術中・術後のデータの記録を時系列に行うデータログシステムの統合を行った．また，そのパフォーマンスの評価を行ったことで，リアルタイム処理を施すことでシステム全体の性能の向上が期待できることがわかった．本研究の一部は“身体機能解析・補助・代替機器開発研究”及び“日本学術振興会未来開拓学術研究推進事業外科領域を中心とする「ロボティクシステムの開発(99I00904)」” による．

参考文献

[1] A.pernozzoli et al: A Real-time CORBA Based System Architecture for Robot Assisted Craniofacial Surgery, Medicine Meets Virtual Reality 2000.

[2]八木昭彦他：CORBA を用いた異種環境統合システムの開発および評価, 第 12 回日本コンピュータ外科学会大会論文集, pp99-100, 2003

Combined compression and elongation experiments and non-linear modelling of liver tissue for surgical simulation

C. Chui[1] E. Kobayashi[1] X. Chen[2] T. Hisada[2] I. Sakuma[1]

[1]Biomedical Precision Engineering Laboratory, Graduate School of Frontier Sciences, The University of Tokyo, Japan
[2]Computational Biomechanics Laboratory, Graduate School of Frontier Sciences, The University of Tokyo, Japan

Abstract—*Uniaxial stress–strain data were obtained from in vitro experiments on 20 porcine livers for compressions, elongations and cycles of compression and then elongation. There were about 70 cylindrical samples, with diameter 7 mm and varying height (4–11 mm). The combined compression and elongation test provide a unified framework for both compression and elongation for applications such as computer-aided surgical simulation. It enable the zero stress state of the experimental liver sample to be precisely determined. A new equation that combined both logarithmic and polynomial strain energy forms was proposed in modelling these experimental data. The assumption of incompressibility was justified from a preliminary Poisson's ratio for elongation and compression at 0.43 ± 0.16 and 0.47 ± 0.15, respectively. This equation provided a good fit for the observed mechanical properties of liver during compression–elongation cycles and for separate compressions or elongations. The root mean square errors were 91.92 ± 17.43 Pa, 57.55 ± 13.23 Pa and 29.78 ± 17.67 Pa, respectively. In comparison with existing strain energy functions, this combined model was the better constitutive equation. Application of this theoretical model to small liver samples and other tissues demonstrated its suitability as the material model of choice for soft tissue.*

Keywords—*Liver tissue, Compression and tensile test, Non-linear elasticity, Mechanical properties, Computer-aided surgery*

Med. Biol. Eng. Comput., 2004, 42, 787–798

1 Introduction

UNDERSTANDING THE biomechanics of the liver is important for developing computer simulations that could assist in the invention of new medical devices and procedures, as well as in surgical pre-treatment, planning and training (HAWKES *et al.*, 2003). The properties of materials are specified by equations. Within certain limits of stress and strain rates, many engineering structural materials can be described by idealised equations, such as those for the Hookean elastic solid. However, most biological materials, including human liver, cannot be described so simply. In this paper, we present our investigation that attempts to determine better constitutive equations for porcine liver tissues from uniaxial compression and elongation experiments.

A constitutive equation describes a physical property of a material. Its derivation should begin with empirical measurements. There are two alternatives for constitutive modelling: the continuum approach and the microstructure approach. With the first approach, the material is assumed to be a continuum. The relevant variables are identified, and these are related in a framework that ensures invariance under a change of frames. This was our approach in this paper.

One of the earliest reported mathematical/experimental treatments of biological materials in the context of large deformation and modern continuum mechanics was that of Ticker and Sacks, in 1964 and 1967, according to VOSSOUGHI (1995). Since then, a number of constitutive models have appeared that described the passive material properties of both hard and soft tissues. However, few deal with abdominal tissues such as the liver. If the material is linear, and the deformation is limited and infinitesimal, then a simple linear relationship according to Hooke's law might be sufficient uniquely to describe the stress–strain relationship. For a non-linear material capable of undergoing large deformations, the formulation is not unique. One constitutive model may well represent one type of soft tissue but not the others, or a model may well approximate

---

Correspondence should be addressed to Dr Cheekong Chui; email: cheekong@miki.pe.u-tokyo.ac.jp

Paper received 27 November 2003 and in final form 28 April 2004
MBEC online number: 20043941

a portion of the stress–strain curve, but not the entire space. The numerical complexity of these non-linear functions is also an issue for interactive computing using currently available computer hardware and software.

In DAVIES *et al.* (1999; 2002) and CARTER *et al.* (2001), the authors described biomechanical modelling with experimental indentations of animal abdominal organs, including liver. Their study assumed that the tissues were isotropic, homogeneous and incompressible. A non-linear constitutive model based on a strain energy polynomial function was used in MILLER (2000) to model liver and kidney. The experimental data were from *in vivo* experiments on Rhesus monkeys (MELVIN *et al.*, 1973). The experiments approximated uniaxial compression under high strain rates typical of car crashes. These non-linear models were numerically complex and not suitable for realistic, fast medical simulation. In BRUYNS and OTTENSMEYER (2002), the authors described *in vitro* testing of rat organ tissue using indentation and utilised the finite element method to derive as initial estimation of Young's modulus for the tissue. A linear elastic model was assumed in this case for fast computation.

Liver is very unique in its micro-anatomy relative to hepatic arterial, portal venous (unique dual-input supply) and hepatic venous blood with interconnecting lobular sinusoidal anatomy. Other organs behave differently when distended with blood under normal vascular pressures. It was necessary to have an in-depth investigation into the biomechanical properties of liver on its own. To date, YAMADA (1970) provides the most popular data on the mechanical properties of animal tissues.

We first describe the theory of non-linear constitutive equations and our framework. A strain energy function was used in the derivation of non-linear constitutive equations from uniaxial experiments. There are also other constitutive equations that have no apparent relationship with energy functions. These tend to be limited to the uniaxial state of stress–strain and, hence, are not reported in this paper. The energy-based equations are generally applicable in multiaxial-based formulations. The common energy functions frequently used by various investigators have polynomial, exponential, power or logarithmic forms. A good survey of the various forms of strain energy equations can be found in VOSSOUGHI (1995).

In this paper, we proposed a new constitutive equation based on a combined polynomial–logarithmic energy function. We discuss our theoretical framework and describe our uniaxial experiments. *In vitro* uniaxial experiments have long been used to characterise the biomechanical properties of living tissues. Tissue samples were extracted and usually subjected to either compression tests or elongation tests. However, we performed combined compression and elongation testing in addition to these conventional tests. In addition to providing the most relevant, unified framework for both compression and elongation for applications such as computer-integrated surgical simulation, this test enables the zero-stress state to be precisely determined.

Based on our experimental data, a comprehensive set of strain energy functions were investigated to determine their suitability for representing the biomechanical properties of liver. Our observations and new model were further validated with separate experiments using smaller liver samples. The new combined logarithmic and polynomial model was also used to model a compression and then elongation experiment on porcine kidney and brain tissues.

2 Theories of non-linear constitutive relationships

A well-known approach for studying non-linear constitutive relationships of bodies capable of finite deformation is to postulate that elasticity has the form of an elastic potential, or strain energy function, W. The strain energy for an elastic body is a function of the state of deformation.

Let X denote a point in the reference configuration. The current position of the point is denoted by x, where x is a function of time. The gradient of x with respect to X is called the deformation gradient

$$F = \left(\frac{\partial x}{\partial X}\right)^T \tag{1}$$

The right Cauchy–Green tensor C is a measure of the strain the body experiences

$$C = F^T F \tag{2}$$

The constitutive assumption of non-linear elasticity is that the stress tensor at point x depends only on the material and the deformation gradient at x. If the mechanical properties do not depend explicitly on the particular point x, the material is said to be homogeneous. We have assumed that liver tissue is homogeneous in our investigation.

When a quantity is unchanged with a frame rotation, it is said to be invariant. From C, which is a second-order tensor, three scalar invariants can be formed by taking the trace of C, C^2 and C^3. They are

$$I = \mathrm{trace}(C) = C_{ii},\ II = \mathrm{trace}(C^2) = C_{ij}C_{ji} \text{ and}$$
$$III = \mathrm{trace}(C^3) = C_{ij}C_{jk}C_{ki}$$

However, it is customary to use strain invariants defined as follows:

$$I_1 = I,\ I_2 = \frac{1}{2}(I^2 - II) \text{ and } I_3 = \frac{1}{6}(I^3 - 3I \cdot II + 2III)$$
$$= \det(C)$$

Assuming that liver is isotropic, the strain energy function can be expressed as a function of the above strain invariants, $W(I_1, I_2, I_3)$. We denote λ_i as the principal values of F, and I_i is a function of λ_i.

$$F = \begin{pmatrix} \lambda_1 & & \\ & \lambda_2 & \\ & & \lambda_3 \end{pmatrix} \tag{3}$$

As liver is known to comprise highly incompressible material, $\det F = \lambda_1\lambda_2\lambda_3 = 1$. Under uniaxial deformation, the cross-sectional area of the cylindrical sample reduces by $1/\lambda$ when the height of the sample is increased by a factor of λ. By setting $\lambda = \lambda_3$, we have $\lambda_1 = \lambda_2 = 1/\sqrt{\lambda_3}$. Invariants I_1, I_2 and I_3 under uniaxial deformation can be evaluated as $I_1 = \lambda^2 + 2/\lambda$, $I_2 = 2\lambda + 1/\lambda^2$ and $I_3 = 1$, respectively.

For an elastic material, the second Piola–Kirchhoff stress tensor S can be expressed in terms of strain energy W and Green–Lagrange strain tensor E as follows:

$$S = \frac{\partial W}{\partial E} = 2\frac{\partial W}{\partial C} \tag{4}$$

The Cauchy stress σ is related to S by

$$\sigma = \frac{1}{J} F \cdot S \cdot F^T \tag{5}$$

where $J = \det F$.

We can now express a component of σ in the tensile or compressive direction as a partial derivative of W by the invariants

$$\sigma = 2\frac{\partial W}{\partial I_1}\left(\lambda^2 - \frac{1}{\lambda}\right) + 2\frac{\partial W}{\partial I_2}\left(\lambda - \frac{1}{\lambda^2}\right) \tag{6}$$

As Cauchy stress σ is related to the first Piola–Kirchhoff stress tensor T by

$$\sigma = \frac{1}{J} F \cdot T \tag{7}$$

we can deduce that $\sigma = \lambda T$.

From (6),

$$T = \frac{2}{\lambda}\frac{\partial W}{\partial I_1}\left(\lambda^2 - \frac{1}{\lambda}\right) + \frac{2}{\lambda}\frac{\partial W}{\partial I_2}\left(\lambda - \frac{1}{\lambda^2}\right) \tag{8}$$

Suppose that the original cross-sectional area of the cylindrical sample used in our experiment is A_0 and the tensile or compressive load is F, then

$$T = \frac{F}{A_0} \tag{9}$$

If the original length of the cylindrical sample is L_0, the displacement

$$\Delta L = L_0(\lambda - 1) \tag{10}$$

T in (9) is measured using a precise instrument described in the following section. The instrument also concurrently measures the displacement in (10). By comparing the experimental curve obtained by plotting T against λ with the theoretical curve from (8), obtained using various strain energy functions, we seek to determine the strain energy function that can best represent the material behaviour of porcine liver tissue.

Strain energy functions have long been proposed for modelling the mechanical behaviour of biological materials and tissues. For solid biomechanics, most of the work has concentrated on blood vessels and myocardium. There are fewer reports of work on lung, skin, ligament, tendon, cartilage and bone tissue. To the best of our knowledge, there is as yet no strain energy-based constitutive relationship that is derived from extensive measurements on liver. Our assumption for the isotropic, homogeneous and incompressible liver model is consistent with recent literature (SCHMIDLIN *et al.*, 1996; FARSHAD *et al.*, 1998; MILLER, 2000; CARTER *et al.*, 2001; DAVIES *et al.*, 2002) on modelling of abdominal organs for surgical simulation.

2.1 *Polynomial strain energy functions*

The Mooney–Rivlin material is an example of a strain energy function with polynomial form (MOONEY, 1940). The Mooney–Rivlin material has been adequate for most qualitative engineering purposes in modelling hyperelastic solids such as rubber.

Using the following Mooney–Rivlin energy function with nine material constants (known as the nine-constant theory),

$$\begin{aligned} W = {} & C_1(I_1 - 3) + C_2(I_2 - 3) + C_3(I_1 - 3)^2 \\ & + C_4(I_1 - 3)(I_2 - 3) + C_5(I_2 - 3)^2 + C_6(I_1 - 3)^3 \\ & + C_7(I_1 - 3)^2(I_2 - 3) + C_8(I_1 - 3)(I_2 - 3)^2 \\ & + C_9(I_2 - 3)^3 \end{aligned} \tag{11}$$

where C_1, C_2, C_3, C_4, C_5, C_6, C_7, C_8 and C_9 are material constants.

We derived the stress–strain relationship from (8). The resulting equation was highly complex, with the highest-order term having a power of 6 and the lowest-order term having a power of -5.

Equation (12) is the two-constant version of the energy function for the Mooney–Rivlin material

$$W = \frac{C_1}{2}(I_1 - 3) + \frac{C_2}{2}(I_2 - 3) \tag{12}$$

where C_1 and C_2 are material constants, and $C_1, C_2 > 0$.

Partial differentiation of W in (12), with I_1 and I_2 obtained from (8), yielded the following stress–strain relationship. Note that λ is equal to strain plus 1. For ease of discussion, we simply refer to $T = f(\lambda)$ as the stress–strain relationship.

$$T = C_1\lambda + C_2 - \frac{C_1}{\lambda^2} - \frac{C_2}{\lambda^3} \tag{13}$$

Using non-linear curve fitting, we could evaluate how well this stress–strain relationship represented the experimental data.

The simplest polynomial-based energy function is the neo-Hookean model, which was originally applied to incompressible non-linear elastic engineering materials. The neo-Hookean model is a subset of the Mooney–Rivlin model with $C_2 = 0$. There is only one material constant C_1 in this equation (14).

$$W = C_1(I_1 - 3) \tag{14}$$

2.2 *Exponential and logarithmic strain energy functions*

Equation (15) is an exponential form of strain energy due to FUNG (1967) and DEMIRAY (1972)

$$W = \frac{C_1}{2C_2}\left(e^{C_2(I_1-3)} - 1\right) \tag{15}$$

where C_1 and C_2 are material constants, and $C_1, C_2 > 0$.

Partially differentiating W in (15) with I_1 and $\partial W/\partial I_2 = 0$, we obtained from (8) the stress–strain relationship.

In VERONDA and WESTMANN (1970), the authors proposed the following energy function:

$$W = C_1\left(e^{C_3(I_1-3)} - 1\right) + C_2(I_2 - 3) + g(I_3)$$

As we assumed that liver tissue is incompressible, $g(I_3) = 0$.

$$W = C_1\left(e^{C_3(I_1-3)} - 1\right) + C_2(I_2 - 3) \tag{16}$$

For cat's skin, VERONDA and WESTMANN (1970) suggested the following values for the material constants: $C_1 = 0.00394$, $C_2 = -0.01985$, $C_3 = 5.03$. Partially differentiating W in (8) with I_1 and I_2, we obtained from (16) the stress–strain relationship.

A related class of exponential equations with logarithmic form was proposed by Hayashi and Takamizawa (TAKAMIZAWA and HAYASHI, 1987; HAYASHI, 1993). They concluded from their investigations that the logarithmic form is far superior to the polynomial form and somewhat better than the exponential form. The equation was intended for transversely anisotropic material. We proposed the following logarithmic equation for isotropic material:

$$W = -C_1 \ln(1 - C_2(I_1 - 3)) \tag{17}$$

The main difference between (17) and the original Hayashi equation is the absence of invariant I_4 in the former. This invariant was not applicable with an isotropic material. We assumed that liver is an isotropic material in this paper. The original equation of Hayashi was listed as

$$W = -C_1 \ln\left(1 - \frac{1}{2}C_2(I_1 - 3)^2 + \frac{1}{2}C_3(I_4 - 1)^2 + C_4(I_1 - 3)(I_4 - 1)\right)$$

2.3 *Equations from power law stress–strain model*

The fourth type of commonly used constitutive relationship is the power law of the form $T = KS^n$, where T is the Lagrangian stress tensor, S is the strain or strain rate tensor, and K and n are the material constants. The advantage of the power law stress–strain function is its simplicity. Equation (18) was originally proposed by TANAKA and FUNG (1974). It was used to model the zero-stress state of blood vessel walls in XIE *et al.* (1995).

$$T = C_1(\lambda - 1)^{C_2} \tag{18}$$

The power law energy function has also been used extensively in mechanical engineering. The Odgen model, as described in HISADA and NOGUCHI (1995), for example, was originally proposed for incompressible, rubber-like materials. In ZOBITZ *et al.* (2001), the extrafibrillar matrix of tendon material was formulated as a hyperelastic material using the Odgen form of strain energy function.

$$W = \sum_{n=1}^{3} \frac{C_n}{\alpha_n}(\lambda_1^{0.5\alpha_n} + \lambda_2^{0.5\alpha_n} + \lambda_3^{0.5\alpha_n})$$

$$T = \sum_{n=1}^{3} \frac{C_n}{2}(\lambda^{\alpha_n} - \lambda^{0.5\alpha_n - 1}) \tag{19}$$

A variant of the Odgen model was proposed in BOGEN (1987) to describe passive myocardial behaviour where C_1 and C_2 are material constants. The equations were as follows:

$$W = \frac{C_1}{C_2}(\lambda_1^{C_2} + \lambda_2^{C_2} + \lambda_3^{C_2} - 1)$$

$$\sigma = C_1(\lambda^{C_2} + \lambda^{-2C_2}) \tag{20}$$

The Cauchy stress σ is related to first Piola–Kirchhoff stress T by (7). Hence, the first Piola–Kirchhoff form of the Bogen equation used in our studies is

$$T = C_1(\lambda^{C_2 - 1} + \lambda^{-2C_2 - 1}) \tag{21}$$

2.4 *Combined energy functions*

We observed in our preliminary investigations that stress–strain equations derived from the polynomial strain energy function could fit the complete compression and elongation cycle. However, these equations generally have higher standard errors compared with exponential functions when used to represent independent compression or elongation. It is therefore meaningful to combine the exponential and polynomial strain energy functions to produce a more representative constitutive equation.

The first reported attempt to apply the combined equation was in FUNG *et al.* (1993). FUNG *et al.* proposed a strain energy expression that combined polynomial and exponential forms. This expression followed from their finding that linear (Hooke's law), exponential and power law models did not fit the entire stress–strain curve obtained from their experiments with canine thoracic aorta. As HAYASHI (1993) reported that the logarithmic form of strain energy function was somewhat better than the exponential form, and our preliminary investigation also revealed that the logarithmic form was indeed better, we focussed on the combined logarithmic and polynomial model here. The application of the combined exponential and polynomial equations is not reported in this paper.

The combined logarithmic and polynomial model can be derived in the same spirit as the derivation in FUNG *et al.* (1993). At low strain, the logarithmic component in the combined model was small, and the polynomial component was the dominant one. Their roles were reversed at high strain. The combined logarithmic and polynomial model is therefore advantageous in describing the entire stress–strain curve. Note that the Veronda and Westmann model (16) also has both exponential and polynomial terms. The Veronda and Westmann model was a sum of an exponential function and a polynomial originally for constitutive modelling of the skin. It did not have the numerical advantages described above from combining the strengths of exponential and polynomial forms. Equation (22) is our proposed combined logarithmic and polynomial equation for isotropic materials

$$W = \frac{-C_1}{2}\ln(1 - C_2(I_1 - 3)) + C_3(I_1 - 3) \tag{22}$$

To simplify the discussion, we have referred to this equation as the combined logarithmic and polynomial model.

3 Materials and methods

The recent interest and progress in measuring the mechanical properties of tissues have been fuelled by developments in computer-integrated surgery, where précise information about the elastic properties of living tissues is desired. Surgical instruments have been equipped with force-sensing capabilities, allowing elasticity measurement during surgery (CARTER *et al.*, 2001; MUTHUPILLAI *et al.*, 1995). PATHAK *et al.* (1998) applied indentation methods for *in vivo* experiments on the skin. However, these techniques lacked well-defined boundary conditions during the experiment and often failed to address the complex material properties of tissue with nonlinear constitutive equations.

MR elastography (KYRIACOU *et al.*, 1996) was a possible method for non-invasive imaging of elastic properties in non-homogeneous organs. This method spatially maps and quantifies small displacements caused by propagating harmonic mechanical waves. Nevertheless, the resulting very small displacements and frequency range could not predict the tissue behaviour in the range of strains and strain rates observed during surgical interventions.

Uniaxial tests have long been used to measure the mechanical properties of both soft and hard tissues (YAMADA, 1970). MILLER and CHINZEI (1997) described a uniaxial compression test to measure the mechanical properties of brain tissue. We reported our preliminary work on uniaxial experiments with porcine liver in SAKUMA *et al.* (2003). Indentation tests were used in DAVIES *et al.* (2002) to determine the mechanical properties of spleen tissue. To simulate the deformation of liver tissue more realistically, we needed precise measurements of the mechanical behaviour from compression and elongation experiments. Hence, in addition to performing the conventional compression and elongation tests on liver tissue, we measured the force-displacement during a cycle of compression and elongation. This combined compression and elongation test also enabled the zero-stress state to be precisely determined for the tension test.

We found that, by compressing a cylindrical liver sample of diameter 7 mm with a force of less than 1 N, we could start the tension test at the zero-stress and -strain state. In our other work on investigating the strength of liver, we found that the yield stress and strain were approximately 2.5×10^5 Pa and 69.5% for compression. With this yield stress, the compressive stress achieved by 1 N was one order of magnitude less than the yield stress. We also found that the resultant force-displacement relationship before and after preconditioning did not change with 1 N of preconditioning load. The combined compression and elongation cycle was clearly a simpler method compared with the use of lasers for initial state estimation (MILLER and CHINZEI, 1997).

Fresh porcine livers were purchased from a local slaughterhouse for these experiments. It is generally believed that the mechanical properties of pig liver are close to those of human liver. The weight of a whole porcine liver was 1.5 ± 0.2 kg. Test samples were cylindrical in shape, with a fixed diameter of 7 mm and heights ranging from 4.5 mm to 11 mm.

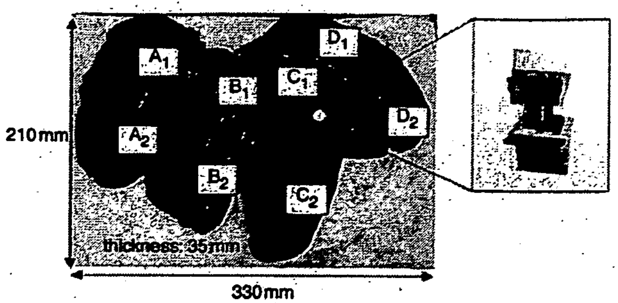

Fig. 1 *Whole porcine liver with test sample. Eight groups of samples were extracted from different locations (A_1, A_2, B_1, B_2, C_1, C_2, D_1, D_2) in liver. Average mass densities at these locations were 1.070, 1.078, 1.030, 1.074, 1.058, 1.074, 1.074 and 1.057 g cm^{-3}, respectively*

Fig. 1 shows a typical whole liver and one of the liver samples used in the experiments. Before testing, samples were visually inspected for visible vessels and large pores. We looked for vessels from all sides of the sample. Those samples with vessels or obvious pores were discarded. As the samples were rather small, at 7 mm diameter, and generally less than 10 mm in height, and because they were extracted near the liver surface, we were quite certain that the presence of a vessel in the sample was not significant, even if missed by the inspection.

The density of porcine liver referred to or implied mass density and was determined by dividing the measured weight of the specimen by its volume. The volume of the cylindrical sample was easily determined, as its radius and height were measured during the preparation. Digital scales were used to weigh the sample before and after the experiments. We assumed that liver tissue was isotropic. A digital video camera was placed in front of the sample and recorded the deformation during the experiment. From the recorded planar images, we calculated the area of the sample, based on the number of pixels. The area remained roughly constant before, during and after the various experiments. The difference in area at any recorded instant of the experiment was at most 2%. As there was no change in weight before and after the experiment, we assumed that the density, and specifically the weight of the liver, did not change before, after and during the various experiments. Additionally, based on a study of 24 elongation and 15 compression experiments, we determined that the Poisson's ratios for elongation and compression were 0.43 ± 0.16 and 0.47 ± 0.15, respectively. Hence, the porcine liver tissue sample was possibly incompressible. This is an important condition for the application of the various energy based constitutive models described in Section 2.

Fig. 2 illustrates the experimental procedure. The tissue sample to be tested was extracted from the pig liver using a disposable surgical knife. Surgical bond* was used to glue the sample to the attachments. To establish maximum bonding between the tissue and the attachment unit, we tested the adhesion between liver tissue and various surfaces, including wood, steel, cloth and rubber. Adhesion to the rubber plate was maintained with the highest tension used in our experiments. This was twice that obtained using wood, which had the lowest value. At a temperature of 20 ± 3°C, the surgical bond was able to sustain a stress of up to 380 kg cm^{-2}.

Force and displacement were measured during the loading test by an Eztest precision instrument†. This instrument had a resolution of ± 1% and could support loading rates ranged from 0.5 to 1000 mm min^{-1}. We used a load cell that was capable of measuring a force up to 20 N. Experiments were performed between August and December 2002, with 70 samples taken from 20 pig livers. Environmental temperature was about 22°C. Humidity was kept between 60% and 70% to prevent drying of the test pieces. In the combined compression and elongation test, the sample was first compressed, returned to its stress-free position and then elongated. Preconditioning with periodical loading and unloading was carried out in all tests.

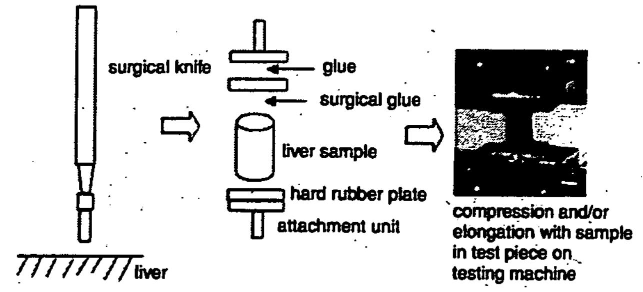

Fig. 2 *Overview of experimental procedure. Sequence flows from left to right. Sample was first extracted from liver surface. Test unit was made and placed under testing machine for experiments*

Note that, from the theoretical treatment above, we refer to stress and strain in the Lagrangian sense. Thus, for a one-dimensional sample loaded in tension, the tensile stress T is the load divided by the cross-sectional area of the sample at zero-stress state. The 'stretch ratio' or 'compression ratio' λ is the ratio of the length or height of the sample stretched or compressed under the load divided by the initial length at the zero-stress state.

For the investigation into the heterogeneity of porcine liver, test sample lengths of 10 ± 1 mm and loading rates of 10 mm min^{-1} were used. Fig. 3 compares the stress–strain curves from the visceral side, diaphragmatic side and edge of the liver. We observed that samples extracted from the upper surface (diaphragmatic side) of the liver were noticeably harder than those from other parts of the liver. This was possibly owing to the presence of a thin capsular layer on the liver surface. As we were mainly interested in computer-aided surgical simulation, with surgical devices such as needles approaching the liver from the top, samples extracted from the

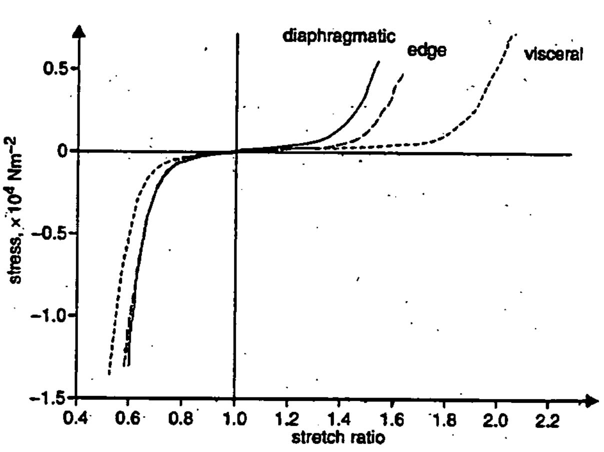

Fig. 3 *Stress–strain relationships for tissue extracted from different parts of liver. Total of 21 samples were extracted from 2 porcine livers. Diameter and height of cylindrical samples were 6–7 mm and 4–5 mm, respectively. Loading rate was 10 mm min^{-1}*

---

*Adhesive A, Sankyo Co. Ltd, Tokyo, Japan

†Shimadzu Co. Ltd, Japan

diaphragmatic side of the liver were used in our biomechanical analyses of liver properties.

We briefly studied the effect of temperature on the mechanical properties of liver. We compared the force-displacement curves obtained at various temperatures (22°C, 37°C and 80°C). At 80°C, the liver tissue was close to vaporisation. The material behaviour of liver tissue was essentially the same at 22°C and 37°C. As we wanted to perform as many tests as possible, experiments were conducted at room temperature (22°C).

Fig. 4 shows the stress–strain relationship of liver tissue obtained at the constant loading rates of 1, 2, 5, 10, 20, 50, 100 and 200 $\mathrm{mm\,min^{-1}}$. These corresponded to strain rates of 0.003, 0.006 0.030, 0.061, 0.151, 0.303 and 0.606 $\mathrm{s^{-1}}$, respectively. The effect of strain rate on porcine liver was shown to be relatively insignificant. Hence, in this investigation, we did not need to consider further the visco-elastic properties of porcine liver.

As has been reported for other animal tissues (FUNG, 1993), porcine liver exhibited tissue relaxation. We observed during these experiments that, when the liver sample was compressed, and then the compression was maintained, the amount of force measured by Eztest gradually decreased. At low loading rates (1–2 $\mathrm{mm\,min^{-1}}$), some tissue relaxation was observed, whereas very fast rates (50–200 $\mathrm{mm\,min^{-1}}$) resulted in large increments between data points. We found that the loading rate of 10 $\mathrm{mm\,min^{-1}}$ was the most suitable. This corresponded to a strain rate of between 0.041 $\mathrm{s^{-1}}$ and 0.015 $\mathrm{s^{-1}}$, as our samples ranged in height from 4 mm to 11 mm. This was consistent with values required for our targeted application, computer-aided surgical simulation, with a low strain rate of 0.01 $\mathrm{s^{-1}}$ reported as typical for neurosurgery. Slightly higher strain rates were included in our study, because we needed to predict the initial response of liver to a surgical probe. In general, higher strain rates occur during abdominal surgery. By testing all samples at the same rate, the confounding effects of the relatively insignificant tissue visco-elasticity were further minimised.

4 Results and discussions

Figs 5–7 show the mean and median stress T against the stretch ratio λ curves corresponding to compression only, elongation only and combined compression and then elongation measurements, respectively. The standard deviation from the mean stress is also indicated in the respective Figure. A constitutive equation in the $T=f(\lambda)$ form is considered to fit the experimental data if the theoretical curve follows the shape of the average curve, and the standard error is small. We defined standard error as root mean square errors (RMSEs), calculated from the difference between the theoretical estimate and the experimental measurement. An error of more than 120 was considered a bad fit. The mismatch between experimental and theoretical curves was apparent with this error. We were seeking to model the entire stress–strain curve in the physiological region, up to values of about 30% strain. Models with few material parameters were preferred for the purpose of computational efficiency. Software for non-linear least-square data fitting using the Gauss–Newton method assisted us in estimating the coefficients for the non-linear functions.

Almost all the constitutive models provided good fits for the experimental data over the elongation region. The fits for the simpler models, the neo-Hookean and the Mooney–Rivlin (two-constants), were not acceptable for fitting the entire curves. The Mooney–Rivlin model with nine constants produced smaller residual errors than its simpler version. This was mainly owing to the higher-order constants. Nevertheless, there were sign changes in the values of material constants in these polynomial-based models.

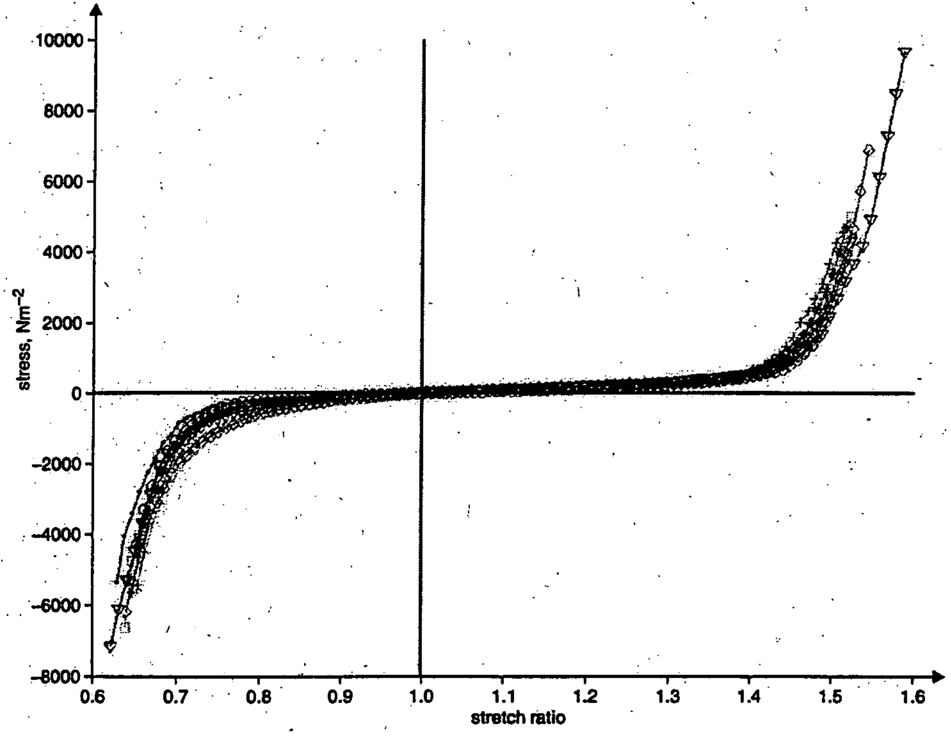

Fig. 4 *Stress–strain relationships for liver tissue obtained at various loading rates. Total of 12 samples were extracted from 1 porcine liver. Diameter and height of cylindrical samples were 7 mm and 5.5 mm, respectively. Loading rates: (–▲–) 1 mm min^{-1}; (–○–) 2 mm min^{-1}; (–+–) 5 mm min^{-1}; (–|–) 10 mm min^{-1}; (–*–) 20 mm min^{-1}; (–□–) 50 mm min^{-1}; (–◇–) 100 mm min^{-1}; (–▽–) 200 mm min^{-1}*

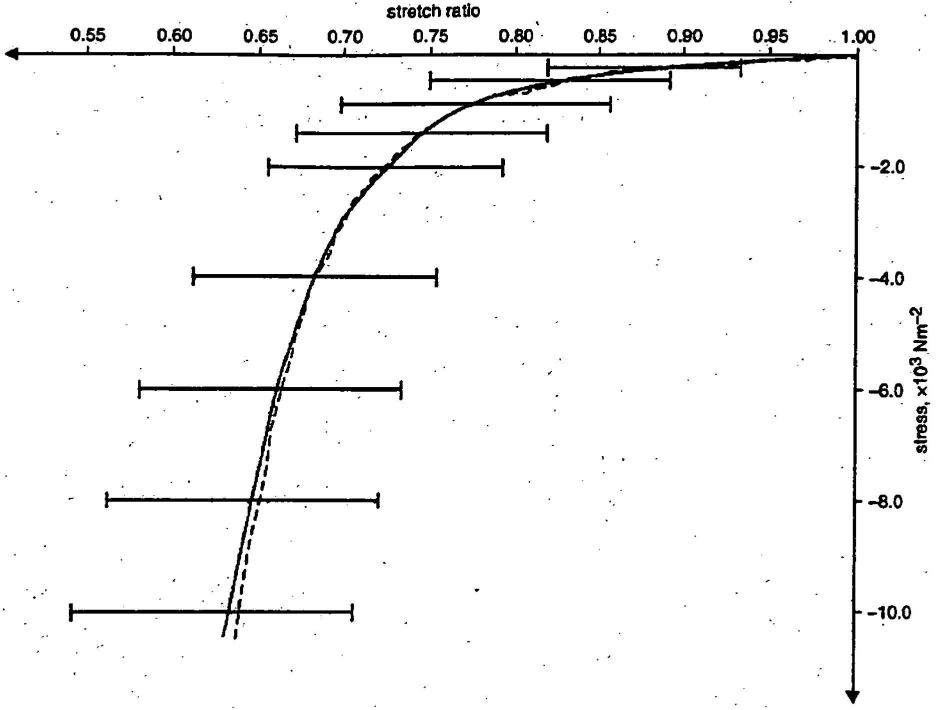

Fig. 5. *Stress (T)–stretch (λ) graphs from uniaxial compression measurements with porcine liver tissue. There were 70 samples from 20 livers. Diameter and height of cylindrical samples were 7 mm and 4–7 mm, respectively. Loading rate was 10 mm min^{-1}. (—) Mean and (—) median values of experiments. Standard deviations from mean values are indicated with horizontal bars*

Both exponential and logarithmic models were comparable in representing the experimental data, with the logarithmic models somewhat better. This is in agreement with previous reports (HAYASHI, 1993). The combined models were better than these models, with respect to their RMSEs. The average error for fitting the maximum, mean and minimum experimental data in the combined logarithmic and polynomial model was 29.78 ± 17.67 Pa. This was the next best after the Mooney–Rivlin (nine-constant) model with 26.63 ± 9.63 Pa.

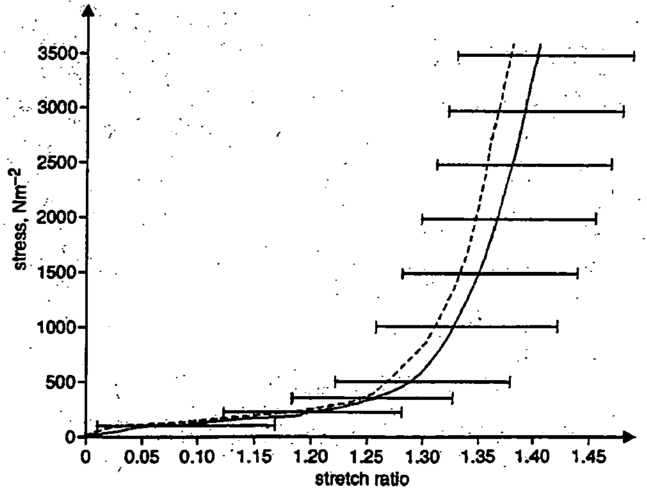

Fig. 6 *Stress (T)–stretch (λ) graphs from uniaxial elongation measurements with porcine liver tissue. There were 11 samples from 4 livers. Diameter and height of cylindrical samples were 7 mm and 8.5–11 mm, respectively. Loading rate was 10 mm min^{-1}. (—) Mean and (- -) median values of experiments. Standard deviations from mean values are indicated with horizontal bars*

The isotropic logarithmic model was third with 46.87 ± 13.74 Pa. The average error of the Veronda and Westmann model and the Fung–Demiray model were 42.91 ± 5.41 Pa and 61.86 ± 9.17 Pa, respectively. The best-fit Mooney–Rivlin (nine-constant) model had the following material constants for minimum, mean and maximum curves, respectively: [-2.97×10^4, 3.14×10^4, -5.36×10^4, 1.32×10^4, 7.86×10^4, 3.23×10^4, 2.34×10^4, -1.10×10^4, -4.45×10^4], [-0.24×10^4, 0.26×10^4, -4.38×10^4, 0.22×10^4, 5.20×10^4, -1.86×10^4, 3.42×10^4, 2.93×10^4, 0.11×10^4] and [0.12×10^4, -0.11×10^4, 5.47×10^4, 0.08×10^4, -6.63×10^4, 3.61×10^4, -2.70×10^4, -3.04×10^4, -3.47×10^4]. The curve fit by the combined logarithmic and polynomial model was achieved using the following material constants for minimum, mean and maximum curve, respectively: [−348.51, 3.03, −328.95], [−337.77, 2.22, −287.78] and [−322.35, 1.51, −210.33].

Not all equations provided good fits for the experimental compression data. The Tanaka model could not match the compression stress–strain curve. In fact, the errors associated with power models were large. Mathematically, a power equation such as the Tanaka model could not represent compression, as the theoretical stress computed using this equation was always positive for all positive stretch ratios. The exponential and logarithmic models were comparable in representing the experimental data. The combined model was good. The Mooney–Rivlin (nine-constant) model had the smallest RMSE. The higher-degree terms of the polynomial function were responsible for the small RMSEs. The average errors for the Mooney–Rivlin (nine-constant) model and combined logarithmic and polynomial model were 48.98 ± 28.69 Pa and 57.55 ± 13.23 Pa, respectively. The average errors of the isotropic logarithmic model, Fung–Demiray model and Veronda and Westmann model were 110.2 ± 58.93, 154.3 ± 115 Pa and 154.9 ± 115 Pa, respectively. The best-fit Mooney–Rivlin (nine-constant) model had the following material constants for minimum, mean and maximum curves,

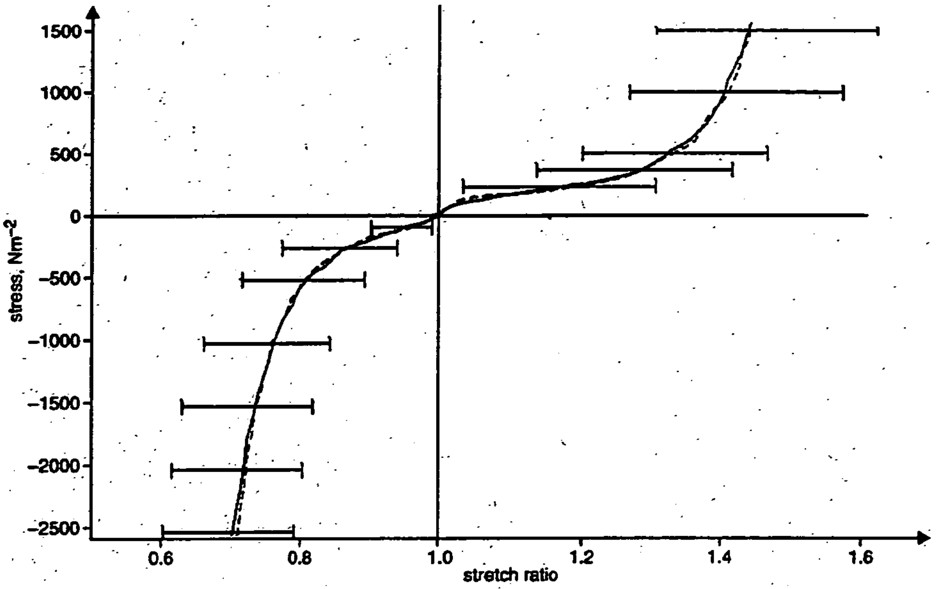

Fig. 7 Stress (T)–stretch (λ) graphs from uniaxial combined compression and elongation measurements with porcine liver tissue. There were 65 samples from 18 livers. Diameter and height of cylindrical samples were 7 mm and 4–7 mm, respectively. Loading rate was 10 mm min^{-1}. (—) Mean and (– – –) median values of experiments. Standard deviations from mean values are indicated with horizontal bars.

respectively: [-1.98×10^4, 1.91×10^4, 5.75×10^4, -0.61×10^4, $7.3.95\times10^4$, 1.18×10^4, 2.72×10^4, 1.42×10^4, -0.33×10^4], [0.03×10^4, 0.0024×10^4, -0.73×10^4, -0.07×10^4, 0.72×10^4, -1.98×10^4, 0.43×10^4, 0.80×10^4, -0.24×10^4] and [-0.27×10^5, 0.26×10^5, 0.96×10^5, -0.09×10^5, -0.91×10^5, 0.28×10^5, 1.09×10^5, 1.45×10^5, -1.21×10^5]. The curve fit by the combined logarithmic and polynomial model was achieved using the following material constants for minimum, mean and maximum curve, respectively: [−6767.58, 1.12, −2812.78], [−7881.10, 1.65, −3941.40] and [−9922.58, 2.42, −5936.80].

Table 1 shows the results of fitting the above constitutive equations to experimental data for compression and then elongation. Failure to match the experimental data (RMSE > 120 Pa) was partly due to the difficulties in representing both negative and positive domains numerically in

Table 1 Parameters of various models representing combined compression and then elongation experimental data. Models were ranked in accordance with average RMSE ± SD

Model	Minimum curve	Mean curve	Maximum curve	Average RMSE ± SD, Pa
Mooney–Rivlin (nine-Constants) (11)	$C_1=0.20\times10^4$ $C_2=-0.15\times10^4$ $C_3=-0.61\times10^4$ $C_4=0.30\times10^4$ $C_5=0.19\times10^4$ $C_6=3.16\times10^4$ $C_7=-3.35\times10^4$ $C_8=-0.76\times10^3$ $C_9=0.55\times10^4$	$C_1=0.16\times10^3$ $C_2=0.14\times10^3$ $C_3=-0.12\times10^4$ $C_4=0.62\times10^3$ $C_5=0.41\times10^3$ $C_6=0.72\times10^4$ $C_7=-1.43\times10^4$ $C_8=0.91\times10^4$ $C_9=-0.92\times10^3$	$C_1=-0.23\times10^4$ $C_2=0.27\times10^4$ $C_3=-0.99\times10^3$ $C_4=0.32\times10^4$ $C_5=-0.15\times10^4$ $C_6=1.03\times10^4$ $C_7=-2.18\times10^4$ $C_8=0.31\times10^3$ $C_9=1.40\times10^4$	38.71 ± 21.99
Combined logarithmic and polynomial (22)	$C_1=-457.21$ $C_2=9.77$ $C_3=-119.78$	$C_1=-342.44$ $C_2=1.99$ $C_3=-136.08$	$C_1=-214.73$ $C_2=4.71$ $C_3=-221.21$	91.92 ± 17.43
TAKAMIZAWA and HAYASHI (1987) (17)	$C_1=752.57$ $C_2=0.61$ $C_3=0.20$ $C_4=0.29$	$C_1=168.01$ $C_2=4.11$ $C_3=0.82$ $C_4=1.17$	$C_1=175.08$ $C_2=9.27$ $C_3=1.27$ $C_4=1.89$	134.6 ± 23.06
BOGEN (1987) (18)	$C_1=-47.87$ $C_2=3.90$	$C_1=-43.98$ $C_2=5.44$	$C_1=-83.553$ $C_2=6.4399$	153.5 ± 50.13
Fung–Demiray (15)	$C_1=525.32$ $C_2=2.618$	$C_1=670.65$ $C_2=4.570$	$C_1=1209.2$ $C_2=6.829$	187.6 ± 87.02
Veronda and Westman (16)	$C_1=99.45$ $C_2=2.62$	$C_1=72.62$ $C_2=4.58$	$C_1=87.56$ $C_2=6.84$	188.2 ± 87.26
Odgen (19)	$C_1=1.58\times10^5$ $C_2=-2.96\times10^5$ $C_3=1.54\times10^5$	$C_1=4.12\times10^5$ $C_2=-7.70\times10^5$ $C_3=4.03\times10^5$	$C_1=5.06\times10^5$ $C_2=-8.23\times10^5$ $C_3=3.78\times10^5$	411.8 ± 39.37

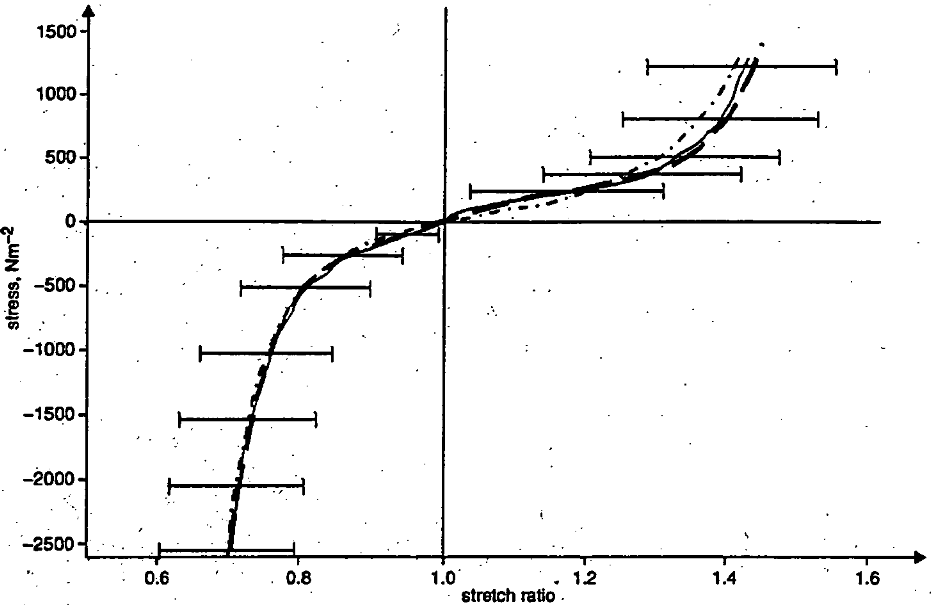

Fig. 8 *Comparison of theoretical and experimental stress (T) stretch (λ) graphs for combined compression and elongation experiments. (—) Mean values of experiments. Standard deviations from mean values are indicated with horizontal bars. (– – –) Theoretical estimation from Mooney–Rivlin (nine-constant) model. (——) Theoretical estimation from combined logarithmic and polynomial model*

some of these equations. Exponential and logarithmic models did fit these data, but with relatively high errors. There was no clear advantage in using exponential or logarithmic forms of equations over high-order polynomial equations. The combined energy model and Mooney–Rivlin (nine-constant) model were the only models that could adequately represent these data. Fig. 8 compares the theoretical estimations from the best-fit Mooney–Rivlin (nine-constant) model and the combined polynomial and logarithmic model with the mean value of the experimental stress–strain data.

Generally, the exponential and logarithmic models represented the stress–strain curves better than the polynomial models during compression or elongation. The polynomial models with adequate orders were preferred for combined compression and elongation over exponential or logarithmic models. However, the best constitutive models appeared to be the ones that combined both logarithmic and polynomial forms. These combined logarithmic and polynomial equations provided a good fit for the stress–strain relationships in the tests involving compression followed by elongation, as well as consistently matching the independent compression and elongation data. This combined model was the next best after the Mooney–Rivlin (nine-constant) model in terms of RMSE. As our objective was to obtain relatively simple constitutive equations for fast computer simulation, the smaller number of material constants required in the combined equation was advantageous. Another disadvantage of the Mooney–Rivlin (nine-constant) model was that its material parameters varied widely: a parameter could be positive in one representation and negative in another. This pitfall was typical of polynomial-based constitutive equations. It could cause very different mechanical behaviour in 3D cases. It would also pose serious accuracy issues during numerical analysis, such as the finite element method (HISADA and NOGUCHI, 1995).

Mean values across samples have been used particularly for analysis involving a large number of samples (MILLER and CHINZEI, 1997; MILLER, 2000). In our study, the results from curve-fitting the average stress–strain curve are consistent with those of individual samples. We defined the median stress–strain curve of a porcine liver as the experimental stress–strain curve that was closest to the median value of all the stress–strain curves obtained with samples from that liver. We curve fitted the median stress–strain curve of six porcine livers with the combined logarithmic and polynomial equation and the Mooney–Rivlin (nine-constants) equation. Table 2 shows the parameters and RMSEs for fitting each individual porcine liver. The RMSEs of each curve fit fall within the range defined earlier for both equations. For the Mooney–Rivlin (nine-constant) model, its material parameters varied widely: a parameter could be positive in one representation and negative in another, which happened in all six porcine liver samples. Hence, in view of the smaller number and more consistent material parameters, the combined logarithmic and polynomial model is indeed the better constitutive model.

To validate further the suitability of the combined logarithmic and polynomial equation, we performed separate experiments with small liver samples. The small liver samples had diameters of only 3 mm. Four test samples from one pig, under the same experimental conditions, were tested. Fig. 9 shows the theoretical results and the average for the experimental results for these tests. The theoretical results obtained using this model agreed with the elongation results using these small liver samples.

We repeated the analyses for liver with porcine kidney and brain tissues. The experimental conditions and procedures were the same for all three types of soft tissue. A close fit was possible with the combined logarithmic and polynomial model. The combined logarithmic and polynomial model could model these tissues with similar errors and small deviations